

1           **Intermittency at Earth's Bow Shock: Measures of**  
2           **Turbulence in Quasi-Parallel and Quasi-Perpendicular**  
3           **Shocks**

4                           **J. Plank<sup>1</sup>, I. L. Gingell<sup>1</sup>**

5                           <sup>1</sup>School of Physics & Astronomy, University of Southampton, Southampton, UK

6           **Key Points:**

- 7           • We examine the evolution of turbulent fluctuations across Earth's bow shock us-  
8           ing magnetic spectra, kurtosis and correlation length.  
9           • The power-law magnetic spectra in the shock transition region are found to be dis-  
10          tinct from the solar wind and magnetosheath.  
11          • The correlation length of high-pass filtered fluctuations shows fast reduction of the  
12          driving scale across a quasi-perpendicular shock.

---

Corresponding author: James Plank, [jp5g16@soton.ac.uk](mailto:jp5g16@soton.ac.uk)

**Abstract**

Turbulent plasmas such as the solar wind and magnetosheath exhibit an energy cascade which is present across a broad range of scales, from the stirring scale at which energy is injected, down to the smallest scales where energy is dissipated through processes such as reconnection and wave-particle interactions. Recent observations of Earth's bow shock reveal a disordered or turbulent transition region which exhibits features of turbulent dissipation, such as reconnecting current sheets. We have used observations from Magnetospheric Multiscale (MMS) over four separate bow shock crossings of varying  $\theta_{Bn}$  to characterise turbulence in the shock transition region and how it evolves towards the magnetosheath. We observe the magnetic spectrum evolving by fitting power laws over many short intervals and find that the power-law index in the shock transition region is separable from that of the upstream and downstream plasma, for both quasi-perpendicular and quasi-parallel shocks. Across the shock, we see a change in the breakpoint location between inertial and ion power-law slopes. We also observe the evolution of scale-independent kurtosis of magnetic fluctuations across the shock, finding a reduction of high kurtosis intervals downstream of the shock, which is more apparent in the quasi-perpendicular case. Finally, we adapt a method for calculating correlation length to include a high-pass filter, allowing estimates for changes in correlation length across Earth's bow shock. In a quasi-perpendicular shock, we find the correlation length to be significantly smaller in the magnetosheath than in the solar wind, however the opposite can occur for quasi-parallel shocks.

**Plain Language Summary**

Turbulence is a phenomenon that can arise in anything that behaves like a fluid under certain conditions. The size and shape of turbulent vortices and eddies can tell us a lot about the energy contained within the fluid. For example, highly energetic particles emitted from the Sun form a turbulent, fluid-like plasma called the solar wind. The Earth's magnetic field acts as an obstacle to the solar wind, forming a shock wave called the bow shock, similar to the shock wave formed by a supersonic jet in air. This shock wave is very complex and introduces an additional source of turbulent structures. In this paper, we looked at the turbulence just before the shock wave, during, and after to learn if its presence fundamentally changes how the energy gets distributed inside a turbulent plasma. We found evidence that turbulence behaves differently in these three areas. In addition, the magnetic field angle relative to the shock wave (i.e. nearly parallel/perpendicular to the shock) also has an effect.

**1 Introduction**

Turbulence is a ubiquitous phenomenon in space plasmas, occurring in systems ranging from star formation (McKee & Ostriker, 2007) to galaxy clusters (Zhuravleva et al., 2014) to planetary magnetospheres (Chasapis et al., 2018) and the solar wind (Alexandrova et al., 2013; Bruno & Carbone, 2013; Kiyani et al., 2015). In collisionless plasmas such as the solar wind, the mechanisms for dissipating energy in turbulence are not well-known (Kiyani et al., 2015), and solving this problem is vital for our understanding of turbulence in general. In the heliosphere, for example, turbulent dissipation is a suggested source of the heating observed in the Solar corona (Cranmer et al., 2015; Klimchuk, 2006). One of several proposed solutions to this dissipation problem is magnetic reconnection (Carbone et al., 1990; Franci et al., 2017), in which local changes in magnetic topology rapidly transfer energy from fields to particles, resulting in particle acceleration and heating (Burch et al., 2016). Some other possible explanations for energy dissipation include wave-particle interactions, driven by cyclotron resonance or kinetic Alfvén waves (Isenberg & Hollweg, 1983; Hollweg, 1999).

One advantage of using the local space environment to study plasma turbulence is that it allows for high-cadence in-situ observation of structures associated with turbulent dissipation, such as reconnecting current sheets. The Magnetospheric Multiscale (MMS) mission has recently been used to observe electron outflow jets at thin current sheets - a signature of reconnection - in Earth's magnetosheath (Phan et al., 2018) and the bow shock transition region (Gingell et al., 2019; Wang et al., 2017). Recent simulations (Bessho et al., 2020, 2022; Gingell et al., 2017; Matsumoto et al., 2015) have shown that processes in the shock foot can generate current sheets and magnetic islands, contributing to the formation of a transition region that can appear turbulent. The properties of turbulence are also known to vary across different plasma regimes, such as the solar wind and magnetosheath (Alexandrova, 2008). Furthermore, the properties of turbulence are also known to vary within the magnetosheath, varying with the upstream shock orientation (Yordanova et al., 2020) and between the sub-solar point and flanks (Huang et al., 2017; Sahraoui et al., 2020). Hence, these observations of turbulence and coherent structures in the shock layer, and differences in the character of turbulence throughout the magnetosheath together raise two open questions: 1) Is there a measurable difference between turbulence seen in the bow shock transition region and in the surrounding plasma (i.e. the solar wind and magnetosheath)? And 2) How quickly does well developed turbulence arise in the magnetosheath after a bow shock crossing? For both of these questions we also compare the differences between quasi-parallel and quasi-perpendicular shocks.

We note that some definitions of turbulence require a ‘well-developed’ inertial range, allowing a complete cascade from the largest, fluid-like scales in the plasma, through the kinetic regime and ending at the dissipation scale. In the shock transition region, disordered fluctuations may be driven by non-linear interactions and instabilities that arise at scales smaller than the inertial range, but nevertheless appear to cascade and dissipate energy in the region. In this study we will refer to these processes as turbulent, however it is possible that they will not always fit the definition of fully developed turbulence.

In this paper, we address the above observations by studying the evolution of magnetic fluctuations from the solar wind to magnetosheath, i.e. across the bow shock, using three different measures of turbulence: the magnetic spectrum, the kurtosis, and the correlation length (e.g. Stawarz et al., 2019). From the magnetic spectrum we extract the spectral break between inertial and ion scale ranges, which is related to local plasma scales such as the ion gyroradius  $\rho_i$ , and inertial length  $d_i$  (Chen et al., 2014; Franci et al., 2015). We found that the magnetic spectrum in the shock transition region was steeper than both upstream and downstream regions at the electron scale in the quasi-perpendicular event. Observing scale independent kurtosis, we saw consistent evidence for intermittency in the solar wind and transition region for both quasi-parallel and quasi-perpendicular shocks, with peak kurtosis in the shock foot. Finally, we use an adapted method of calculating correlation length to measure the local stirring scale of the turbulence, and find significant differences between upstream and downstream plasma. Addressing the time taken to reach well developed turbulence, Kolmogorov-like spectral power laws arise in the inertial range approximately 30s (or  $1.6R_E$ ) downstream of the shock in the quasi-perpendicular case, while for the quasi-parallel shock the time is closer to 2 minutes ( $6.2R_E$ ). However, the correlation length transitioned almost instantaneously across the shock for the quasi-perpendicular shock, but took 1 – 2 minutes for the quasi-parallel shock.

## 2 Data Set

We explore the bow shock transition using in situ data obtained by the Magnetospheric Multiscale (MMS) mission (Burch et al., 2015). Magnetic field data are provided by the fluxgate magnetometer (FGM) (Russell et al., 2014) and search coil magnetometer (SCM) (Contel et al., 2014). FGM and SCM data are analysed as a merged data set (FSM) (Argall et al., 2018). Particle data are provided by the Fast Plasma Investigation's

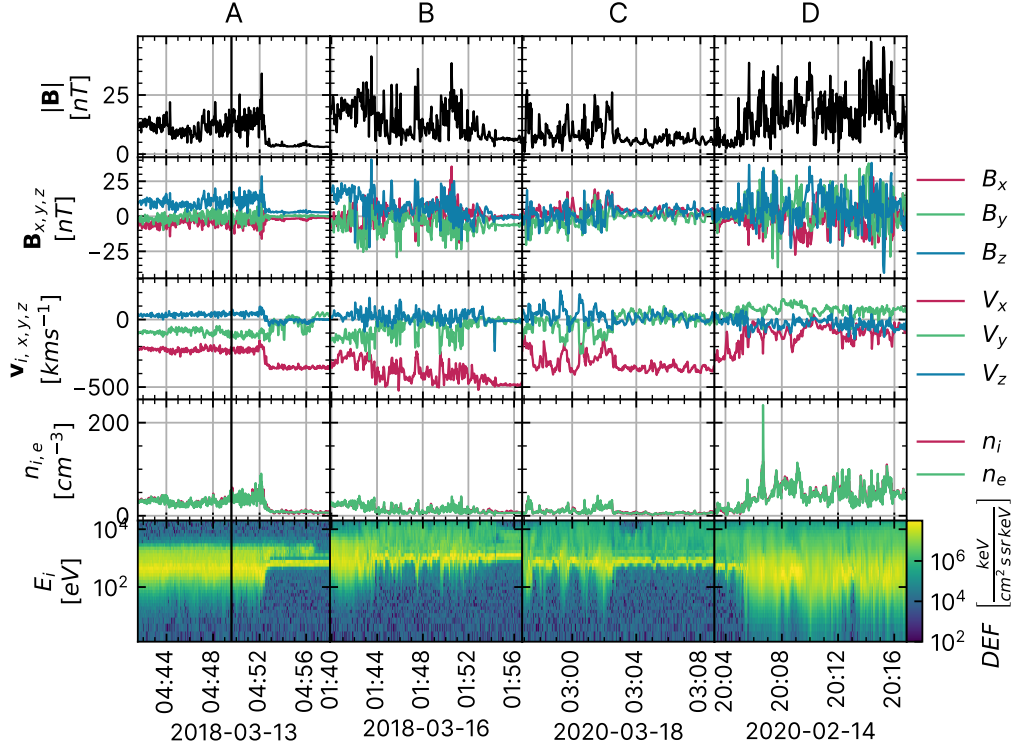


**Figure 1.** MMS observations showing events A (left column), and D (right column). Row 1: Magnetic field strength,  $|\mathbf{B}|$ ; Row 2: Magnetic field components,  $\mathbf{B}$ , in GSE coordinates; Row 3: Ion velocity components,  $v_i$  (GSE); Row 4: Proton and electron densities,  $n_{i,e}$ ; Row 5: Ion energy spectrogram. In events A-C, MMS travels from magnetosheath to solar wind, and in event D MMS travels from solar wind to magnetosheath. The shock normal angles are  $\theta_{Bn} = 68^\circ, 41^\circ, 35^\circ, \& 33^\circ$  for A and D respectively. The timestamp of Figure 3 is indicated by a vertical black line in the left column.

114 (FPI) (Pollock et al., 2016) Dual Electron Spectrometer (DES) and Dual Ion Spectrom-  
 115 eter (DIS). In high-resolution burst mode, the SCM and FSM magnetic fields are avail-  
 116 able at a sampling cadence of  $f_s = 1/8192$  s, while FGM is available at  $1/128$  s. Par-  
 117 ticle moments are available at a cadence of 0.15 s and 0.03 s for ions and electrons, re-  
 118 spectively.

119 Four high-resolution (burst) bow shock crossing intervals have been analysed here.  
 120 The events were chosen to cover a range of bow shock angles from quasi-perpendicular  
 121 to quasi-parallel, where the burst interval was longer than approximately 10 minutes. Event  
 122 D was found with the help of a database of 2797 shocks compiled using machine learn-  
 123 ing, from Lalti et al. (2022). These four shocks were chosen firstly due to the intervals  
 124 each recording sufficient burst data both upstream and downstream of the shock, allow-  
 125 ing us to observe the evolution. Secondly, they all performed well on the test of Taylor’s  
 126 hypothesis, described further in section 2.1. Figure 1 provides a summary of events A  
 127 and D, the most parallel and most perpendicular of the four events studied. The inter-  
 128 vals on 13 March 2018, 16 March 2018, 18 March 2020 and 14 February 2020 are referred  
 129 to as intervals A, B, C and D respectively. Note that electron moments are not available  
 130 for MMS 4 during event D. All events are  $\sim 15$  minutes in duration. Table 1 shows  
 131 plasma parameters averaged over the entire upstream interval, including electron upstream  
 132 flow speed  $v_0$ , the acute angle between upstream magnetic field,  $\mathbf{B}$ , and the shock nor-  
 133 mal,  $\theta_{Bn}$ , Alfvén Mach number  $M_A$  of the upstream flows, and the ion plasma beta  $\beta_i$ .  
 134 The derived parameters  $M_A$  and  $\beta_i$ , along with observed values for  $v_0$  and the magnetic  
 135 field, were obtained from OMNI (King, 2005). The shock angle  $\theta_{Bn}$  was calculated us-  
 136 ing a model from Peredo et al. (1995), using the upstream magnetic field lagged to the  
 137 bow shock from OMNI and FPI moments from MMS. Sample standard errors on the an-  
 138 gles were low for each of the events, with a maximum of  $\pm 3.0^\circ$  for event B.

139 The angle between the upstream magnetic field and shock normal angle,  $\theta_{Bn}$ , de-  
 140 creases from quasi-perpendicular ( $68^\circ$ ) in event A to quasi-parallel ( $33^\circ$ ) in event D. Quasi-  
 141 perpendicular shocks are characterised by near discontinuous transitions from the solar  
 142 wind to bow shock. In contrast, a quasi-parallel shock has a more gradual transition and  
 143 can often be complicated by upstream waves and instabilities caused by backstreaming  
 144 ions in the foreshock. Therefore, the expectation is that structures created by the shock  
 145 are more distinct in quasi-perpendicular shock crossings but are only observed for a short  
 146 time, whereas a quasi-parallel shock will display complex behaviour that is more chal-  
 147 lenging to separate from the solar wind or magnetosheath.

**Table 1.** Average upstream plasma properties as observed by OMNI and MMS. Data from OMNI were averaged over the same duration as MMS.

Interval	$\theta_{Bn} [^\circ]$	$v_0 [km.s^{-1}]$	$M_A$	$\beta_i$	Start yyyy/mm/dd hh:mm:ss	End
A	$68 \pm 0.6$	$356.4 \pm 1.0$	$14.6 \pm 1.1$	$4.4 \pm 0.7$	2018/03/13 04:41:33	04:58:02
B	$41 \pm 3.0$	$475.8 \pm 4.7$	$9.0 \pm 0.7$	$1.4 \pm 0.3$	2018/03/16 01:39:53	01:56:43
C	$35 \pm 1.1$	$394.4 \pm 3.9$	$9.8 \pm 0.8$	$2.2 \pm 0.5$	2020/03/18 02:56:53	03:08:52
D	$33 \pm 0.8$	$330 \pm 2.4$	$14.6 \pm 0.3$	$1.1 \pm 0.9$	2020/02/14 20:03:13	20:16:52

148 **2.1 Validity of Taylor’s Hypothesis**

149 The interpretation of results in Section 3 relies on the validity of transforming the tem-  
 150 poral domain measurements from MMS1 into the spatial domain, assuming the Taylor  
 151 hypothesis. The assumption is that fluctuations will travel past the spacecraft at a bulk

152 flow speed  $v_0$  that is much greater than the wave propagation speeds, thus the spatial  
 153 configuration of the fluctuations is unchanging as they are swept past the spacecraft. For  
 154 plasmas with a fast flow speed,  $v_0 \gg v_A$ , such as the solar wind, this assumption is  
 155 well founded. However, for plasmas such as the magnetosheath and the bow shock Tay-  
 156 lor’s hypothesis may not be valid.

157 The increments of the magnetic field,  $\delta\mathbf{B}$ , are given by:

$$\delta\mathbf{B}(\tau) = \langle |\mathbf{B}(t + \tau) - \mathbf{B}(t)| \rangle_T \quad (1)$$

158 where  $\tau$  represents the time lag, and  $\langle \rangle_T$  represents the mean over the full time interval.  
 159 The lag  $\tau$  can be transformed into spatial lag  $\ell$  according to Taylor’s hypothesis using  
 160 the bulk flow speed:  $\ell = v_0 t$ . In this case,  $v_0$  is the mean bulk velocity in each region  
 161 (solar wind, bow shock or magnetosheath).

162 We can also measure the magnetic field increments for spatial lag  $\ell$  directly using  
 163 the separation between spacecraft pairs, without needing to assume Taylor’s hypothe-  
 164 sis. The equation in this case is then:

$$\delta\mathbf{B}(\ell_{ij}) = \langle |\mathbf{B}^i(t) - \mathbf{B}^j(t)| \rangle_T \quad (2)$$

165 where  $i, j = 1, 2, 3, 4$  are labels for each of the four spacecraft, then  $ij$  indicates one  
 166 of the six spacecraft pairs, and  $\mathbf{B}^i$  indicates the magnetic field vector as measured by  
 167 spacecraft  $i$ . We are therefore able to test the validity of Taylor’s hypothesis by direct  
 168 comparison of the amplitude of the magnetic field increments for single and multi-spacecraft  
 169 measures. However, the nature of this test means that comparisons can only be made  
 170 for scales close to the separation of the six MMS pairs. Therefore, good performance of  
 171 this test at the spacecraft separation scales does not necessarily guarantee good perfor-  
 172 mance at larger or smaller spatial scales.

173 We assess the validity of Taylor’s hypothesis separately in each of the three regions  
 174 (upstream, shock and downstream) for events A and D here, in Figure 2, with correspond-  
 175 ing plots for events B and C shown in the supplementary material, Figure S1. Figure  
 176 2 shows magnetic fluctuation amplitude normalised to average field strength,  $|\delta\mathbf{B}|/B_0$ ,  
 177 for both single spacecraft and for the six spacecraft pairs (as in Chen & Boldyrev, 2017).

178 We found that all events performed reasonably well at the available spacecraft sep-  
 179 aration scales, particularly in the magnetosheath. The shock transition in event A sees  
 180 the fluctuation amplitude slightly underestimated, indicating that the structure of the  
 181 plasma is rapidly evolving in this region. In the solar wind in event A, it appears the plasma  
 182 encountered by MMS 1 and 2 compared to MMS 3 and 4 was slightly different, leading  
 183 to two different groups of single spacecraft lines. Chasapis et al. (2017) showed that there  
 184 can be some variation in the second order structure function at the MMS separation scale  
 185 when comparing single and multi spacecraft methods, even for intervals of pure solar wind.  
 186 We will therefore not discount intervals where performance in the solar wind is not per-  
 187 fect. Event D performs best overall with single spacecraft measurements in all regions  
 188 being very close to the multi spacecraft results.

### 189 3 The Magnetic Spectrum

190 In order to examine the evolution of the magnetic spectrum, events A-D were split  
 191 into consecutive, non-overlapping windows containing 6 seconds of data per window. There  
 192 are 145, 112, 79, and 133 windows for each event A-D, resulting in  $N \approx 4 \times 10^4$  FSM  
 193 field measurements per window, along with 40 ion measurements and 200 electron mea-  
 194 surements. The power spectrum of  $\mathbf{B}$  in the spacecraft frame is given as,  $PSD(\mathbf{B}, k)$ ,

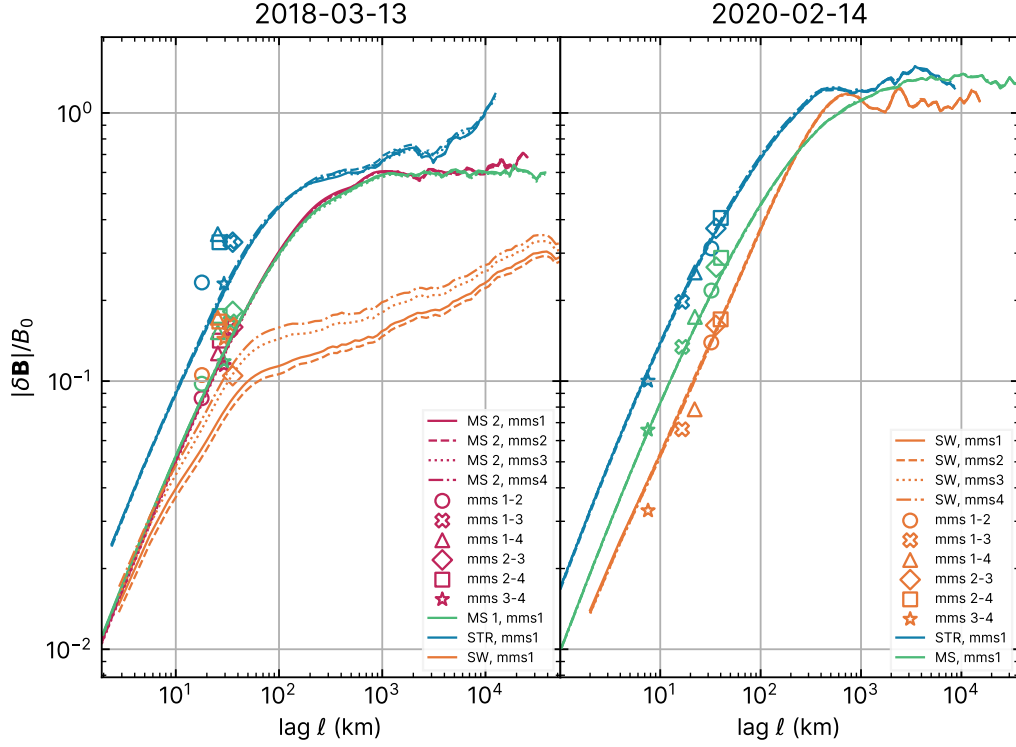


**Figure 2.** Magnetic fluctuation amplitude normalised to average field strength,  $|\delta\mathbf{B}|/B_0$  as a function of scale  $\ell$ . *Left:* Event A, *right:* event D. Fluctuation amplitude obtained using a single spacecraft and assuming Taylor’s hypothesis is given by a line, solid for MMS 1, dashed for MMS 2, dotted for MMS 3, and dot-dashed for MMS 4. Colours represent the different regions of each event: Orange for solar wind (SW), blue for shock transition region (STR), and green/red for the magnetosheath (MS). Measurements from the six spacecraft pairs, with  $\ell$  equivalent to the separation scale, are shown by the following markers: Circle for MMS 1-2, cross for 1-3, triangle for 1-4, diamond for 2-3, square for 2-4, and star for 3-4. In event A the single spacecraft and multi spacecraft results are reasonably similar, particularly in the magnetosheath. The results for event D are also extremely close at all scales and for all regions.

195 where  $k = 2\pi f/v_0$ ,  $v_0$  is the average flow speed in each region and  $f$  is a discrete fre-  
 196 quency increment in the range  $N/f_s \leq f \leq f_s/2$ . The transformation of frequency  $f$   
 197 to wavenumber  $k$  is performed assuming Taylor's hypothesis, which is discussed in-depth  
 198 in section 2.1. We calculate the trace power spectrum of the magnetic field, where compo-  
 199 nents  $B_{x,y,z}$  are pre-filtered with a Hanning window, and we take the sum of the power  
 200 in the three components i.e.  $P = \sum_i P(B_i)$ .

201 In turbulent plasmas, the magnetic spectrum often appears as a series of power laws  
 202 with varying indices,  $P \propto k^\alpha$  (Frisch, 1995). For example, power-law index  $\alpha = -5/3$   
 203 corresponds to the inertial range of fluid turbulence (Kolmogorov, 1941), typical of space  
 204 plasmas at spatial scales far above ion kinetic scales. At the ion scales,  $\sim d_i$  or  $\sim \rho_i$ , so-  
 205 lar wind and magnetosheath plasmas typically exhibit a breakpoint below which the mag-  
 206 netic spectrum steepens. In this ion kinetic range, the power-law index  $\alpha$  is variable, though  
 207  $\alpha \approx -2.8$  is typical for the solar wind (Alexandrova et al., 2009; Sahraoui et al., 2010).  
 208 The breakpoint between the fluid MHD scale and the ion kinetic scale has been seen at  
 209 the larger of  $d_i$ , or  $\rho_i$  (Chen et al., 2014) when observing solar wind undisturbed by the  
 210 bow shock. A second breakpoint is often observed at electron kinetic scales, and again  
 211 the slope of the magnetic spectrum is expected to steepen in the electron kinetic range,  
 212 below  $\sim d_e$ . Hence, the magnetic spectrum is expected to comprise three or more dis-  
 213 tinct power laws with different slopes. In order to characterise the power laws of our ob-  
 214 served magnetic spectra, we seek an algorithm that can generate and fit an arbitrary num-  
 215 ber of straight lines to a spectrum, with a variable number of breakpoints. Hence, we  
 216 use the Multivariate Adaptive Regression Splines (MARS) algorithm, developed by (Friedman,  
 217 1991), and implemented by (Milborrow et al., 2011). Additionally, the MMS noise floor  
 218 was found to be reached at wavenumbers of approximately  $k \approx 10 \text{ km}^{-1}$ , therefore the  
 219 spectra at  $k \geq 10 \text{ km}^{-1}$  has been excluded from the MARS fit. This was found to sig-  
 220 nificantly reduce the effect of the noise floor, although it does appear in some windows  
 221 as spectral indices  $\geq 0$  at the largest  $k$ .

222 Figure 3 shows an example of a spectrum obtained when MMS was downstream  
 223 of the shock during event A, with the resultant MARS fit overlaid. Examples from the  
 224 solar wind and magnetosheath, and for event D can be found in the supplementary ma-  
 225 terial as Figure S2. We also note that an electron scale wave is visible at  $k \approx 2 \text{ km}^{-1}$   
 226 as a peak in the spectrum. Similar structures appear in other intervals and are charac-  
 227 terised by a dramatic change from positive to negative power law index at the electron  
 228 scale. This demonstrates that the MARS method is able to identify spectral features as-  
 229 sociated with wave activity, and allow interpretation of them separately from the back-  
 230 ground turbulent spectrum.

231 Figures 4 and 5 show the evolution of spectral index with time for the intervals A  
 232 and D, respectively. Equivalent plots are given for events B and C in the supplemental  
 233 material, Figures S3 and S4. Each 6 second window is represented as a vertical slice where  
 234 the spectral index at a given scale is represented by the colour of the vertical bar. The  
 235 extent in  $k$  over which that scale applies is given by the height of the bar, with each slice  
 236 in time usually having 3 or more distinct slopes covering the observed spectrum.

237 In Figure 4, we see that in the solar wind immediately preceding the shock, the break-  
 238 point between the inertial (MHD) range and the ion (kinetic) range is much less than  
 239 both  $d_i$  and  $\rho_i$ . As in Figure 3 above, this observation differs from studies, e.g. Chen et  
 240 al. (2014), who suggest that in undisturbed solar wind, the spectral break should be  $d_i$   
 241 or greater. However, in the magnetosheath close to the shock, we find that the break-  
 242 point shifts to larger scales and settles in the expected range  $d_i \leq BP \leq \rho_i$ . This is  
 243 most likely due to the lack of clean, undisturbed solar wind very close to the bow shock.

244 For event D, Figure 5, the spectral slope in the solar wind is much steeper than ex-  
 245 pected at spatial scales larger than the ion inertial length, with  $\alpha \sim -4$  on average.  
 246 This feature may be caused by an upstream wave for which the peak wavelength is greater

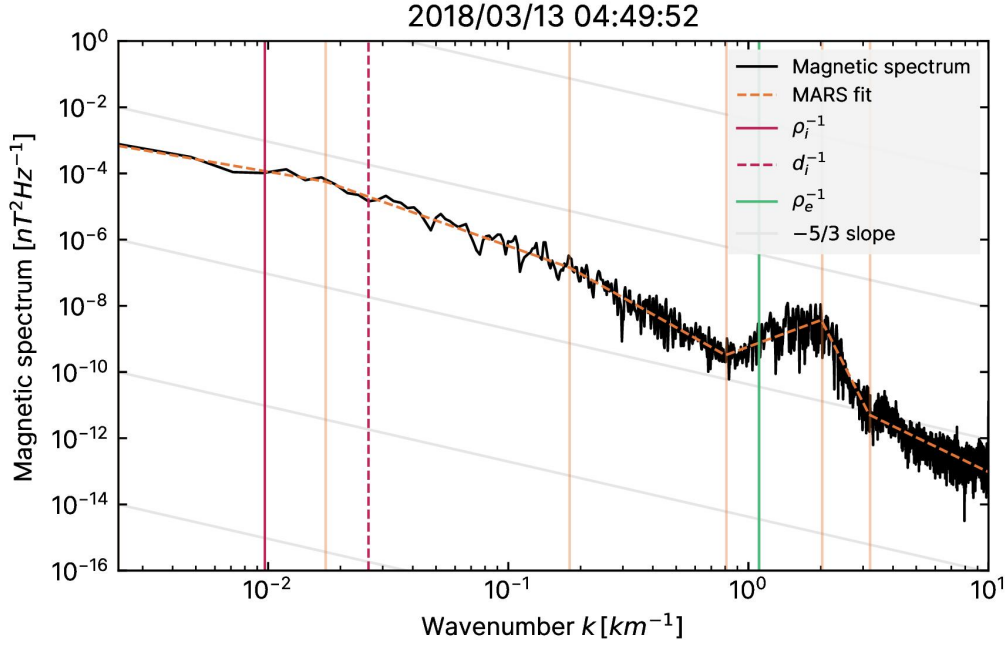


**Figure 3.** A plot of magnetic spectrum for an example  $\sim 6$  s window downstream of the shock on 13/03/2018, illustrated as a vertical black line on Figure 1. Grid lines are shown with a slope of  $-5/3$ . The magnetic spectrum is shown in black. The ion and electron scales ( $\rho_{i,e}$  and  $d_i$ ) are shown as red and green vertical lines. The fit to the spectrum is shown as an orange dashed line, built from chained linear regressions using the MARS method. Vertical orange lines highlight breakpoints determined by the MARS fit. An electron scale wave is visible at approximately  $k \approx 2/\rho_e$ , and this is reflected in the MARS fit by steep upward and downward slopes. The part of the spectrum which exceeds the noise floor at  $k \approx 10 km^{-1}$  has been excluded from this plot.

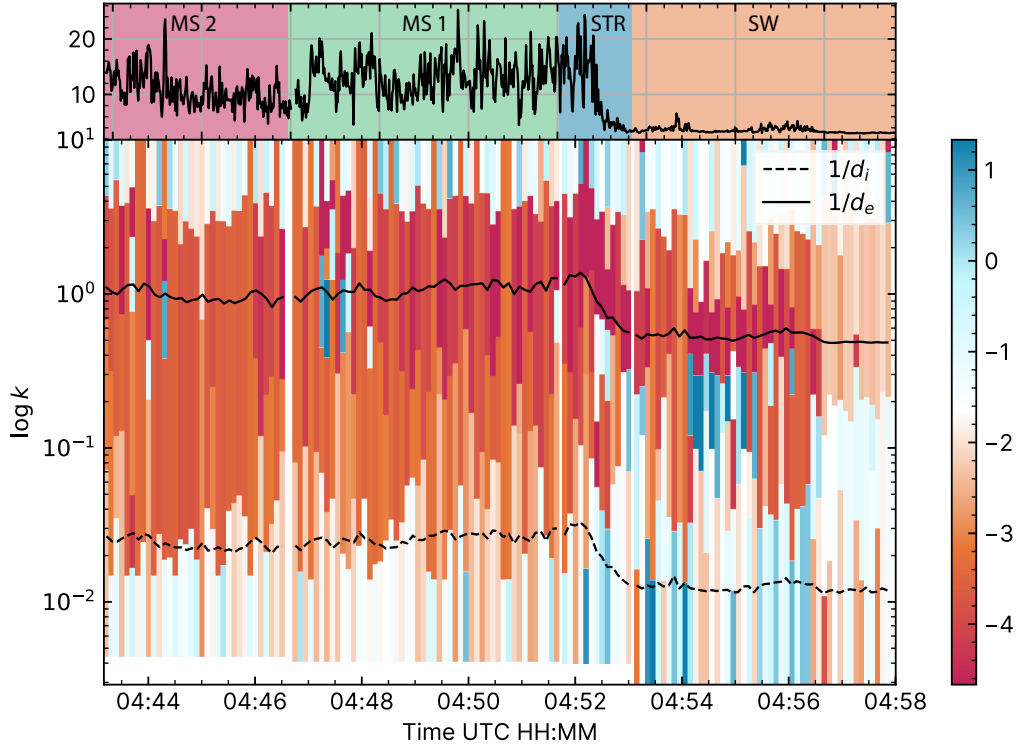


**Figure 4.** Evolution of spectral slopes as a function of time for event A. *Top:* Magnetic field strength,  $|\mathbf{B}|$ . Colours refer to magnetosheath (MS 1/2), shock transition region (STR) and solar wind (SW) *Bottom:* Evolution of spectral indices from MARS fit. Note that this does not always split the spectrum into three regions. The colour represents the slope of the power-law fit. Red indicates steeper than  $-5/3$ , while blue is shallower than  $-5/3$ . Breakpoints are indicated by a change in colour. Electron scales,  $\rho_e \approx d_e$  are shown as a solid black line, and ion scales  $d_i$  and  $\rho_i$  are dashed and dot-dashed black lines. Event A is a quasi-perpendicular shock and as a result we get a clear distinction between solar wind and magnetosheath spectra. The ion-inertial breakpoint (BP) is  $k \gg 1/d_i$  in the solar wind and rapidly transitions to  $1/d_i > k > 1/\rho_i$  in the magnetosheath.

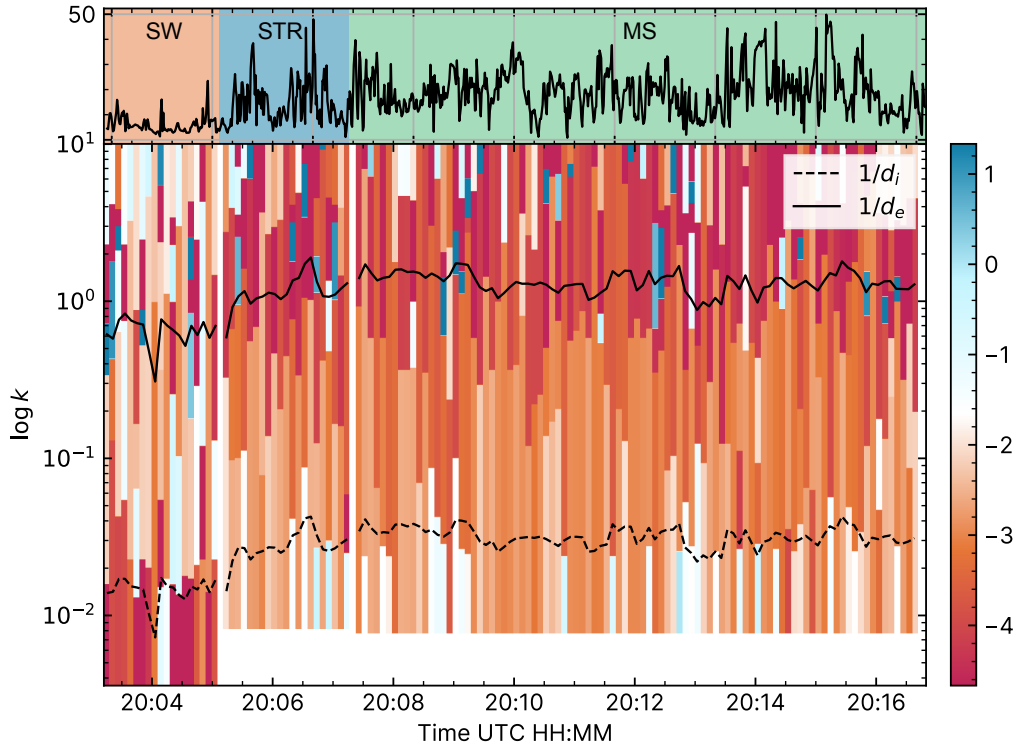


**Figure 5.** Equivalent to Figure 4 for interval D, 20/03/2020. There are many windows where the breakpoint is aligned with  $1/d_i$  throughout the whole event. In the magnetosheath the breakpoints move from shallower to steeper with increasing  $k$ , but in the solar wind the opposite is true and the spectrum is steeper when  $k < 1/d_i$ .

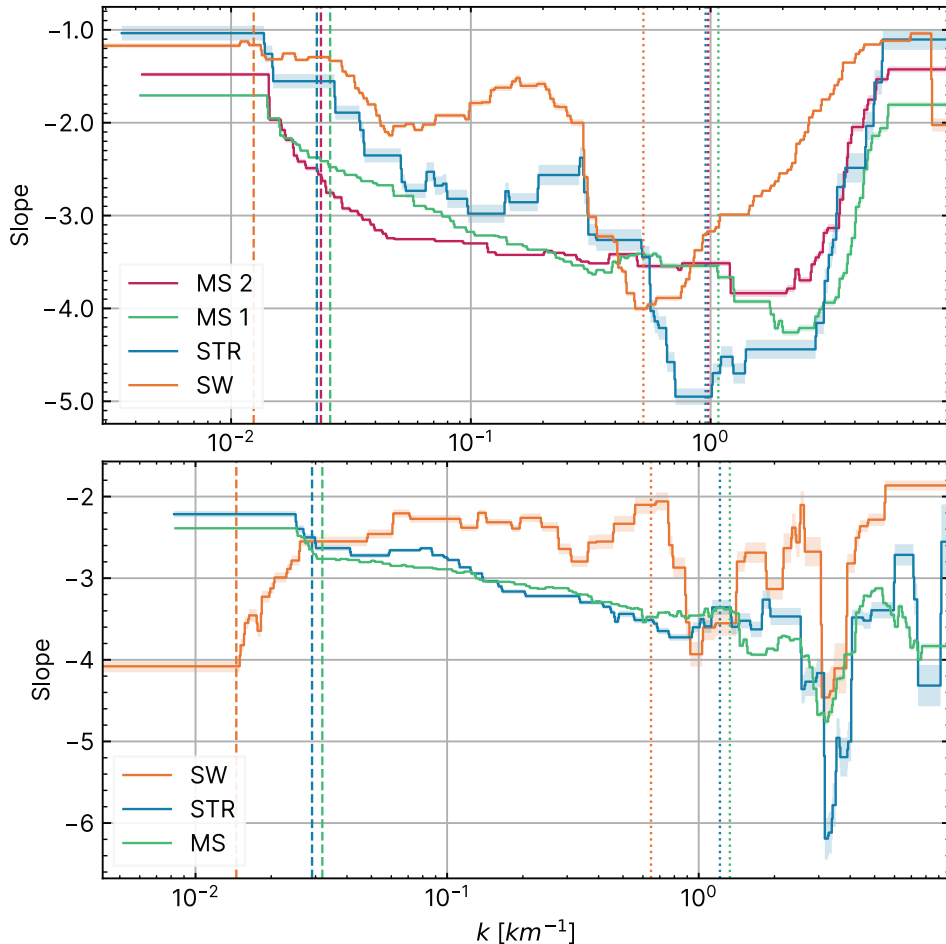


**Figure 6.** Average slope as a function of scale for event A (quasi-perpendicular), *top*, and event D (quasi-parallel), *bottom*. Each line represents a subsection of the entire interval, i.e. magnetosheath (MS - red or green), the shock transition region (STR - blue), or solar wind (SW - orange). The ‘MS 2’ line is further downstream than ‘MS 1’. See Figures 4 and 5 for a definition of the boundaries. Average kinetic scales,  $d_i$  and  $d_e$ , are also plotted as dashed and dotted vertical lines, respectively. We see that there are occasions in both panels where the STR spectral index lies outside of the transition between SW and MS.

247 than the maximum resolvable within each 6s window. This steep spectral slope is not  
 248 observed in the shock transition or magnetosheath. Downstream of the shock, the break-  
 249 point between inertial and ion scales tracks well with  $d_i$  for most windows. In the inertial  
 250 range, we observe a steady spectral slope of  $\alpha \sim -5/3$  approximately 1 minute  
 251 after the spacecraft crosses the shock ramp.

252 Figure 6 shows the average slope as a function of scale,  $k$ , for intervals A and D,  
 253 broken down into subsections based on MMS’s location in relation to the shock, e.g. mag-  
 254 netosheath (MS), in the shock transition region (STR), or the solar wind (SW). The cho-  
 255 sen intervals corresponding to each region are shown in the top panels of Figures 4 and  
 256 5.. Similar figures for intervals B and C are given in the supplemental material, Figures  
 257 S5 and S6. Errors shown are sample standard deviations from all windows within the

258 region. For a ‘quiet’ boundary layer that introduces no new fluctuations to the medium,  
 259 and instead is simply a superposition of modes either side, we might expect the spectral  
 260 slope within that boundary to be between the slope either side. For such a shock, the  
 261 slope in the STR would be between those in the SW and MS at all scales. That is, we  
 262 would see the blue line (slope in the STR) between the green (MS) and yellow (SW) lines  
 263 at all scales, as this would indicate that it is purely a transitional state as solar wind plasma  
 264 crosses the shock and into the magnetosheath. However, we expect the shock to intro-  
 265 duce new waves and instabilities. This is apparent for the given events where the STR  
 266 slope is outside of the MS and SW lines. In event A, we see this most prominently at  
 267 electron scales ( $k \approx d_e$ ), whereas for event D, this occurs at  $k \approx 3d_e$ . We also note  
 268 the extremely steep slope in the inertial range for the solar wind in event D, which was  
 269 also visible in Figure 5. However, for most scales the shock transition region lies between  
 270 the SW and MS lines, or very close to the MS. The source of the steeper shock transi-  
 271 tion region at electron scales could be due to similar scale instabilities or other non-turbulent  
 272 fluctuations at the shock, or an indication of a more efficient turbulent energy dissipa-  
 273 tion process.

274 Comparing the average slopes in Figure 6 to recent statistics from Li et al. (2020)  
 275 of the magnetosheath close to the bow shock at MHD and sub-ion scales, we find that  
 276 event A compares well in both regions, and event D agrees with statistics in the sub-ion  
 277 range. In event A the slope in the MHD range is  $\sim -1.7$ , compared to  $-1.47 \pm 0.24$   
 278 found by Li et al. (2020) for quasi-perpendicular shocks. In the sub ion range the slope  
 279 is  $\sim -3.3$  at the midpoint between  $\rho_i$  and  $\rho_e$ , compared to  $-2.97 \pm 0.65$ . For event D  
 280 the MHD slope is  $\sim -2.2$  compared to  $-1.46 \pm 0.38$ , while for sub-ion scales the slope  
 281 is  $\sim -3.1$  at the midpoint, compared to  $-2.84 \pm 0.15$  from Li et al. (2020). This shows  
 282 that Event A is a more ‘typical’ quasi-perpendicular shock while event D has steeper slopes  
 283 at both MHD and sub ion scales than might be expected for a typical quasi parallel shock.  
 284

## 285 4 Kurtosis

286 A fundamental method for studying intermittency is to examine deviations from  
 287 Gaussianity in the distribution of magnetic field fluctuations, for which a typical method  
 288 is to use the kurtosis (Matthaeus et al., 2015). Intermittency is defined as strong, highly  
 289 localised gradients, especially at small scales. If the kurtosis  $\kappa(\mathbf{B}) > 3$ , then the mag-  
 290 netic field has an overabundance of extreme gradients relative to a normal distribution,  
 291 which therefore indicates the existence of intermittent structures.  $\kappa \leq 3$  indicates that  
 292 intermittency is not present.

293 Figure 7 shows the kurtosis, independent of scale, for events A and D. Events B  
 294 and C are shown in the supplemental material as Figures S7 and S8. The kurtosis is cal-  
 295 culated for consecutive windows containing  $10^5$  samples, based on the rule of thumb  $p_{max} = \log N - 1$ ,  
 296 where  $p_{max}$  is the maximum moment (i.e. fourth) and  $N$  is the number of samples (Dudok  
 297 de Wit et al., 2013). In event A, we see a clear difference in kurtosis between the solar  
 298 wind and magnetosheath. Intermittency is present upstream of the shock, but there are  
 299 very few occasions where  $\kappa > 3$  in the downstream. The kurtosis peaks to over 20 a  
 300 few seconds after the spacecraft crosses the shock ramp into the solar wind in event A.  
 301 In event D, we see the kurtosis peaking in the solar wind before the shock transition re-  
 302 gion, but the peak is much lower at  $\sim 6$ , about one quarter of the peak in event A. Fol-  
 303 lowing the shock there is a period of Gaussian kurtosis ( $\kappa \sim 3$ ), and even some times  
 304 where the distribution is platykurtic ( $\kappa < 3$ ). However, the kurtosis does begin to in-  
 305 crease again further into the magnetosheath. This could be due to motion of the shock  
 306 front towards the spacecraft, causing a partial crossing.

307 In order to directly compare the prevalence of intermittent fluctuations across the  
 308 shock, we next examine the difference between the proportion of bins with  $\kappa > 3$ . For

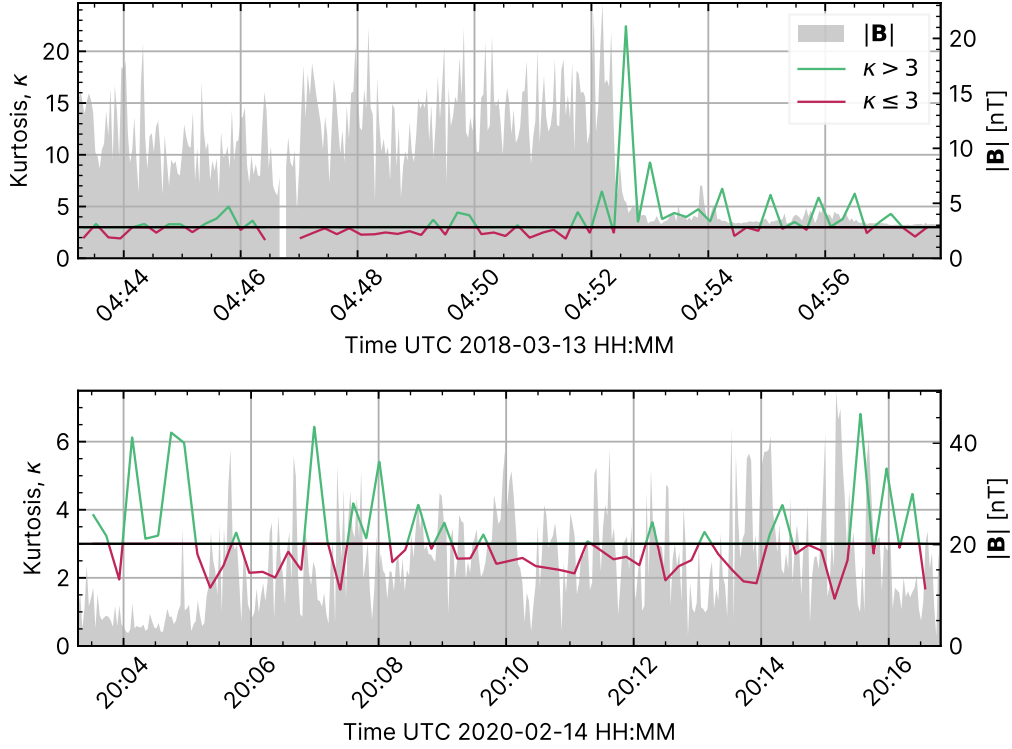


**Figure 7.** Kurtosis examined for events A (*top*) and D (*bottom*).  $\kappa > 3$  is shown green, and  $\kappa \leq 3$  is red. A horizontal black line highlights  $\kappa = 3$ .  $|B|$  is displayed for reference as a grey shaded background, with the vertical scale on the right. The quasi-perpendicular event A shows a clear difference between solar wind and magnetosheath, with  $\kappa$  peaking in the shock foot. The quasi-parallel example (event D) shows a similar relationship, however towards the end of the interval  $\kappa$  begins increasing again.

309 event A, we find that there is a large change across the shock: In the solar wind 60.7%  
 310 of bins show signs of intermittency, whereas 31.8% of bins do in the magnetosheath. For  
 311 quasi parallel event D we observe a lower proportion of intermittent intervals in the up-  
 312 stream, with 50.0% in the solar wind, and a similar proportion to event A, 31.4%, in the  
 313 magnetosheath.

314 Therefore, in comparing the kurtosis observed in quasi-parallel and quasi-perpendicular  
 315 shocks, we find that there are significant changes between the upstream and downstream  
 316 distributions. The solar wind close to the shock and the shock foot have significantly higher  
 317 kurtosis than the magnetosheath. This is visible in both the quasi-parallel and quasi-perpendicular  
 318 case. However, the peak kurtosis is significantly higher for the quasi-perpendicular event  
 319 by a factor of approximately 4.

## 320 5 Correlation Length

321 Next, we seek to measure the characteristic size of turbulent fluctuations in the mag-  
 322 netic field. Energy is typically transferred in a ‘cascade’ from large to small scales on av-  
 323 erage, generating magnetic structures at sizes ranging from stirring scales to the scales  
 324 at which energy is dissipated. The correlation length,  $\lambda_c$ , quantifies the average size of  
 325 the largest scale fluctuations visible in the data (Stawarz et al., 2019, 2022) which can

326 be associated with the ‘stirring’ scale, providing the dataset covers a portion of space  
 327 significant enough for large correlation lengths to be observed. Using the autocorrelation  
 328 function of magnetic fluctuations, given by:

$$R(l) \equiv \frac{\langle \text{Tr}[\delta\mathbf{b}(\mathbf{x} + l)\delta\mathbf{b}(\mathbf{x})] \rangle}{\langle |\delta\mathbf{b}|^2 \rangle}, \quad (3)$$

329 We define the correlation length as follows:

$$\lambda_c \equiv \int_0^\infty R(l) dl. \quad (4)$$

330 Where  $\text{Tr}[\dots]$  is the trace,  $\delta\mathbf{b} \equiv \mathbf{B} - \langle \mathbf{B} \rangle$  and  $l$  is the lag of the autocorrelation.  
 331 This calculation is achieved by integration up to the first zero crossing of  $R(l)$ , or by a  
 332 fit of the form  $R(l) \propto \exp(-l/\lambda_c)$ . We find that results do not differ significantly be-  
 333 tween methods, and we therefore present results using the integration method.

334 Correlation length generally relies on having a data set long enough for a correla-  
 335 tion function to become uncorrelated. However, the region of space near the bow shock  
 336 is a rapidly changing environment dominated by processes unrelated to turbulence. Care  
 337 is therefore needed when selecting what scale of fluctuations should be included. Any  
 338 window of time that includes the shock will have a correlation length that is closely re-  
 339 lated to the crossing time of the shock.

340 In this case, it is more descriptive to examine fluctuations at scales smaller than  
 341 the step-function introduced to the time series by the shock. Therefore, we use a vari-  
 342 able high-pass filter over the event to remove the effect of low frequency variations, such  
 343 as the shock ramp. A 10<sup>th</sup> order Butterworth filter was used, which can be defined by  
 344 the critical frequency,  $F_{crit} \equiv 1/T_{max}$  where  $T_{max}$  is the longest time allowed by the  
 345 filter. By varying  $T_{max}$ , the data is limited exclusively to fluctuations with wavelength  
 346 shorter than  $v_0/2F_{crit}$ . If  $T_{max}$  is less than the period associated with the stirring scale  
 347 of the turbulence, then the measured  $\lambda_c$  will have a dependence on the size of the filter,  
 348 increasing in proportion to  $T_{max}$ . When  $T_{max}$  becomes greater than the period associ-  
 349 ated with the stirring scale,  $\lambda_c$  will appear to plateau, and changes in  $T_{max}$  will not have  
 350 a significant effect on  $\lambda_c$ . Filtering  $\lambda_c$  in this manner provides information on coherence  
 351 scales at, crucially, scales  $\leq T_{max}$ . I.e. With this method we do not capture coherence  
 352 at large scales, most notably in the solar wind. However in the bow shock and magne-  
 353 tosheath, as well as in foreshock structures, we find that this method works well.

354 Similar to the approach used when discussing the magnetic spectrum, we have split  
 355 the interval into smaller consecutive windows. The range of  $T_{max}$  was chosen to cover  
 356 several decades in duration, and are approximately logarithmically spaced. The entire  
 357 event is filtered according to  $T_{max}$  before being split into windows. Figure 8 describes  
 358 the evolution of the frequency-dependent correlation length for event A. Plateaus -  
 359 areas without a significant change in colour between adjacent  $T_{max}$  bins - indicate that a  
 360 consistent correlation length has been reached. We see that in the solar wind, a consis-  
 361 tent  $\lambda_c$  is not reached; the maximum observed correlation length is over  $100d_i$ . However,  
 362 if burst data was available further into the solar wind we would likely have seen this in-  
 363 crease far higher, given that solar wind correlation lengths have been measured by the  
 364 ACE spacecraft at the L1 Lagrange point to be  $0.03 - 0.08AU$ , which is approximately  
 365  $50 - 100 \times 10^3 d_i$  (Ragot, 2022). In the magnetosheath we see a very clear plateau of  
 366  $3 - 10d_i$  immediately downstream of the shock, which appears to slowly increase fur-  
 367 ther into the magnetosheath. At the point in the magnetosheath furthest from the shock  
 368 (04 : 42), the correlation length may still be in a plateau but with  $\lambda_c > 10d_i$ .

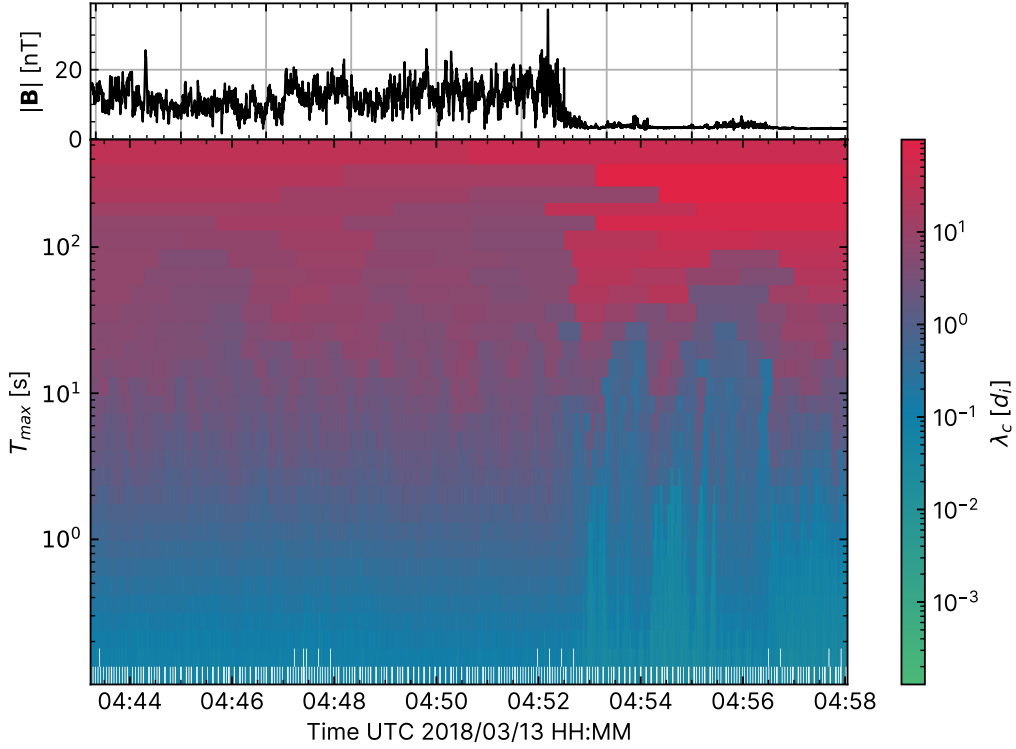


**Figure 8.** *Upper:* Magnetic field strength,  $|B|$ . *Lower:* Correlation length,  $\lambda_c$ , colour (units of ion inertial length), as a function of time and  $T_{max}$ . The width of each bin is equal to  $T_{max}$  up to  $T_{max} = \text{total interval length}/2$ . A plateau, which can be seen in areas where the colour ( $\lambda_c$ ) does not change significantly when moving up to a larger  $T_{max}$ , indicates that the fluctuations are correlated on scales equal-to or smaller-than  $T_{max}$ . There is an observable difference in  $\lambda_c$  before and after the shock; a large plateau exists between  $\lambda_c = 3$  and  $\lambda_c = 10$  immediately downstream of the shock, but in the region upstream of the shock transition region  $\lambda_c$  exceeds  $100d_i$ .

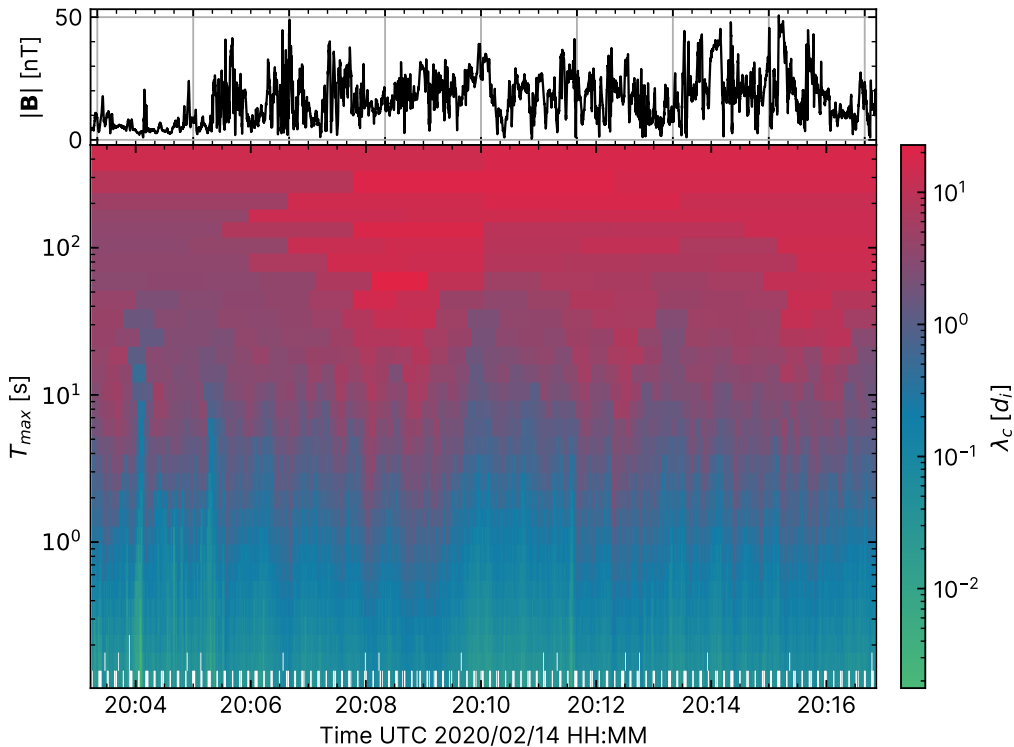


**Figure 9.** Similar to Figure 8 for event D. In this event, correlation length appears to increase on the magnetosheath side.

369 Figure 9 shows an equivalent plot for the quasi-parallel event, D. The correlation  
 370 length on the SW side is approximately  $\lambda_c = 3 - 10d_i$ . There is a foreshock structure  
 371 at 20:04 UTC which may be a partial shock crossing. This indicates that this may not  
 372 be representative of the solar wind, and is instead an extended shock transition region  
 373 or foreshock. These structures may reduce the average correlation length, similar to Fig-  
 374 ure 8. The correlation length after the shock also appears to be in the range  $\lambda_c =$   
 375  $10-12d_i$ , approximately the same as what is observed for the quasi-perpendicular event  
 376 A. These correlation lengths can be compared to recent results from Stawarz et al. (2022),  
 377 who found that  $\lambda_c \approx 10s$  of  $d_i$  at the sub solar magnetosheath, gradually increasing  
 378 to  $100s$  of  $d_i$  in the flanks. For the shocks analysed here, MMS entered the sheath in or  
 379 close to the sub solar region, therefore our results are consistent.

380 Finally, there are indications that shock micro-structure and non-stationarity may  
 381 also have an effect on the correlation length. In the quasi-perpendicular case, Figure 8,  
 382 we see two periods of upstream wave activity visible at 04:54 and 04:56 in the top panel,  
 383 both approximately sixty seconds in duration. This causes a significant reduction of  $\lambda_c$   
 384 of approximately a factor of 10 compared to the immediate surroundings, but only for  
 385  $T_{max} \leq 60s$ . Similar structure is also visible to a lesser extent within the shock ramp  
 386 at 04:52:30. These upstream wave packets may be partial crossings of the shock foot caused  
 387 by ripples on the shock surface (Johlander et al., 2016). Hence, the features in the fil-  
 388 tered correlation length may be associated with fluctuations in the foot and ramp arising  
 389 from this form of non-stationarity. They also appear at larger scales (longer  $T_{max}$ )  
 390 further from the shock, and smaller scales (shorter  $T_{max}$ ) closer to the shock, which is  
 391 perhaps evidence of structures transitioning from larger to smaller scales as the solar wind  
 392 plasma approaches the shock. A similar effect is visible in Figure 9, where periods of large

393 magnetic field amplitude are associated with lower correlation length than the surround-  
 394 ings. However, they are shorter in duration, and we do not observe a reduction in cor-  
 395 relation length closer to the shock. The occurrence of these structures would suggest the  
 396 presence of narrow band waves generated in the shock transition region.

## 397 6 Conclusions

398 In this study, we used three different measures of turbulence, the magnetic spec-  
 399 trum, scale-independent kurtosis and correlation length, to explore the evolution of the  
 400 solar wind and magnetosheath turbulence across Earth's bow shock. The influence of  
 401 the bow shock transition region on the properties of turbulence is not currently well un-  
 402 derstood. Therefore, by using the magnetic spectrum to observe differences in the tur-  
 403 bulent energy cascade, the kurtosis to explore the properties of intermittency and the  
 404 correlation length to describe changes in coherence scales, we aim to produce a repre-  
 405 sentative picture of how turbulence evolves from the solar wind, across the bow shock,  
 406 and downstream into the magnetosheath. We therefore address the following questions:  
 407 1) Is there a measurable difference between turbulence seen in the bow shock transition  
 408 region and in the surrounding plasma? And 2) How quickly does well developed turbu-  
 409 lence arise in the magnetosheath after a bow shock crossing?

410 We find that the shock transition region displays features in the spacecraft frame  
 411 magnetic spectrum that are different to the turbulence present in the solar wind and mag-  
 412 netosheath. This can be seen as shock transition spectral slopes which are steeper at  
 413 scales where  $k \geq d_e$  than either of their upstream or downstream neighbours (Figure  
 414 6). This suggests shock processes are driving scale dependent energy dissipation at sub-  
 415 electron scales. This is observed at both quasi-parallel and quasi-perpendicular shocks  
 416 (events A and D,  $\theta_{Bn} = 68^\circ$  and  $33^\circ$  respectively). However, we note that these sig-  
 417 natures are not always so clearly observable, which is the case for events B and C. Fig-  
 418 ures showing structure (or lack thereof) in the magnetic spectral indices and scale-independent  
 419 kurtosis are shown for events B and C in the supplemental material. We find that the  
 420 breakpoint ( $BP$ ) separating the inertial range from the ion range transitions from  $BP \ll$   
 421  $d_i$  before the shock, to  $d_i \leq BP \leq \rho_i$  in the magnetosheath.

422 Finally, we have adapted the definition of correlation length to include a high-pass  
 423 filter defined by a critical frequency  $F_{crit}$ , which allowed us to calculate a turbulent cor-  
 424 relation length across the shock that effectively removes the large-scale spectral influence  
 425 of the shock. We found that close to the shock the correlation length is longer on the  
 426 solar wind side than the magnetosheath side. Plateaus in high-pass filtered correlation  
 427 length averaged  $25d_i$  in the solar wind and  $< 20d_i$  in the magnetosheath. This relates  
 428 to a reduction in size of the stirring scale in the magnetosheath when compared to so-  
 429 lar wind close to the shock. We found that upstream structures in the shock transition  
 430 region introduce plateaus of reduced correlation length for short periods of time, on the  
 431 order of 10s of seconds.

432 The magnetic spectrum transitioned from solar wind-like to magnetosheath-like over  
 433 a 20s interval for event A and a 1 minute interval for event D. This corresponds to  $180d_i$   
 434 and  $1.1R_E$  for event A, and  $600d_i$  and  $3.1R_E$  for event D. Additionally, the intermittency  
 435 (kurtosis  $\kappa > 3$ ) seen in the upstream transitioned to the average magnetosheath (non-  
 436 intermittent) level after 30s ( $267d_i$  or  $1.7R_E$ ) in the quasi-perpendicular case, whereas  
 437 for the quasi-parallel shock, intermittency was still present until two minutes ( $1.2 \times$   
 438  $10^3d_i$  or  $6.2R_E$ ) after the shock crossing. With regards to the correlation length, the quasi-  
 439 perpendicular case demonstrated a rapid ( $\sim 6s$ ) transition from solar wind-like scales  
 440 to magnetosheath-like scales on crossing the shock ramp. In the quasi-parallel case, how-  
 441 ever, the transition was much slower, occurring over a period of approximately 2 min-  
 442 utes. Together these results suggest that the time needed for the turbulent fluctuations  
 443 to fully develop after crossing the shock ramp is dependent on  $\theta_{Bn}$

444 We note that the case studies shown here may not be representative of all shocks.  
 445 The natural next step is therefore to determine whether the conclusions reached here  
 446 are representative of the typical quasi-parallel or quasi-perpendicular shock. In a future  
 447 work, we will compile a statistical survey of shocks across a range of shock normal angles  
 448 and other plasma parameters, to explore the average behaviour of the bow shock.  
 449 Additionally, we will explore the applicability of these methods to simulations.

## 450 Acknowledgments

451 J. Plank was supported by STFC studentship ST/V507064/1 (2502298). I. L. Gingell  
 452 was supported by the Royal Society University Research Fellowship No. URF\R1\191547.

453 The data that support the findings of this study are openly available at the MMS  
 454 Science Data Center at the Laboratory for Atmospheric and Space Physics (LASP) hosted  
 455 by the University of Colorado, Boulder (<https://lasp.colorado.edu/mms/sdc/public/>),  
 456 references (Burch et al., 2015; Ergun et al., 2014; Lindqvist et al., 2014; Torbert et al.,  
 457 2014; Pollock et al., 2016), and NASA/GSFC's Space Physics Data Facility's OMNIWeb  
 458 service (<https://omniweb.gsfc.nasa.gov/>, references (Lepping et al., 1995; Ogilvie  
 459 et al., 1995; Smith et al., 1998; McComas et al., 1998)).

## 460 References

- 461 Alexandrova, O. (2008, February). Solar wind vs magnetosheath turbulence and  
 462 alfvén vortices. *Nonlinear Processes in Geophysics*, *15*(1), 95–108. Retrieved  
 463 from <https://doi.org/10.5194/npg-15-95-2008> doi: 10.5194/npg-15-95-  
 464 -2008
- 465 Alexandrova, O., Chen, C. H. K., Sorriso-Valvo, L., Horbury, T. S., & Bale, S. D.  
 466 (2013, August). Solar wind turbulence and the role of ion instabilities. *Space Sci-*  
 467 *ence Reviews*, *178*(2-4), 101–139. Retrieved from [https://doi.org/10.1007/  
 468 s11214-013-0004-8](https://doi.org/10.1007/s11214-013-0004-8) doi: 10.1007/s11214-013-0004-8
- 469 Alexandrova, O., Saur, J., Lacombe, C., Mangeney, A., Mitchell, J., Schwartz,  
 470 S. J., & Robert, P. (2009, October). Universality of solar-wind turbulent  
 471 spectrum from MHD to electron scales. *Physical Review Letters*, *103*(16).  
 472 Retrieved from <https://doi.org/10.1103/physrevlett.103.165003> doi:  
 473 10.1103/physrevlett.103.165003
- 474 Argall, M. R., Fischer, D., Le Contel, O., Mirioni, L., Torbert, R. B., Dors, I., ...  
 475 Russell, C. T. (2018). *The fluxgate-searchcoil merged (fsm) magnetic field data*  
 476 *product for mms*.
- 477 Bessho, N., Chen, L.-J., Stawarz, J. E., Wang, S., Hesse, M., Wilson, L. B.,  
 478 & Ng, J. (2022, April). Strong reconnection electric fields in shock-  
 479 driven turbulence. *Physics of Plasmas*, *29*(4), 042304. Retrieved from  
 480 <https://doi.org/10.1063/5.0077529> doi: 10.1063/5.0077529
- 481 Bessho, N., Chen, L.-J., Wang, S., Hesse, M., Wilson, L. B., & Ng, J. (2020, Septem-  
 482 ber). Magnetic reconnection and kinetic waves generated in the earth's  
 483 quasi-parallel bow shock. *Physics of Plasmas*, *27*(9), 092901. Retrieved from  
 484 <https://doi.org/10.1063/5.0012443> doi: 10.1063/5.0012443
- 485 Bruno, R., & Carbone, V. (2013). The solar wind as a turbulence laboratory. *Liv-*  
 486 *ing Reviews in Solar Physics*, *10*. Retrieved from [https://doi.org/10.12942/  
 487 lrsp-2013-2](https://doi.org/10.12942/lrsp-2013-2) doi: 10.12942/lrsp-2013-2
- 488 Burch, J. L., Moore, T. E., Torbert, R. B., & Giles, B. L. (2015, May). Magne-  
 489 tospheric multiscale overview and science objectives. *Space Science Reviews*,  
 490 *199*(1-4), 5–21. doi: 10.1007/s11214-015-0164-9
- 491 Burch, J. L., Torbert, R. B., Phan, T. D., Chen, L.-J., Moore, T. E., Ergun,  
 492 R. E., ... Chandler, M. (2016, June). Electron-scale measurements of  
 493 magnetic reconnection in space. *Science*, *352*(6290). Retrieved from  
 494 <https://doi.org/10.1126/science.aaf2939> doi: 10.1126/science.aaf2939

- 495 Carbone, V., Veltri, P., & Mangeney, A. (1990, August). Coherent structure  
496 formation and magnetic field line reconnection in magnetohydrodynamic turbu-  
497 lence. *Physics of Fluids A: Fluid Dynamics*, 2(8), 1487–1496. Retrieved from  
498 <https://doi.org/10.1063/1.857598> doi: 10.1063/1.857598
- 499 Chasapis, A., Matthaeus, W. H., Parashar, T. N., Fuselier, S. A., Maruca, B. A.,  
500 Phan, T. D., ... Strangeway, R. J. (2017, July). High-resolution statistics of  
501 solar wind turbulence at kinetic scales using the magnetospheric multiscale  
502 mission. *The Astrophysical Journal*, 844(1), L9. Retrieved from [https://](https://doi.org/10.3847/2041-8213/aa7ddd)  
503 [doi.org/10.3847/2041-8213/aa7ddd](https://doi.org/10.3847/2041-8213/aa7ddd) doi: 10.3847/2041-8213/aa7ddd
- 504 Chasapis, A., Matthaeus, W. H., Parashar, T. N., Wan, M., Haggerty, C. C., Pollock,  
505 C. J., ... Burch, J. L. (2018, March). In situ observation of intermittent dissipa-  
506 tion at kinetic scales in the earth's magnetosheath. *The Astrophysical Journal*,  
507 856(1), L19. Retrieved from <https://doi.org/10.3847/2041-8213/aaadf8>  
508 doi: 10.3847/2041-8213/aaadf8
- 509 Chen, C. H. K., & Boldyrev, S. (2017, June). Nature of kinetic scale turbulence in  
510 the earth's magnetosheath. *The Astrophysical Journal*, 842(2), 122. Retrieved  
511 from [https://doi.org/10.3847/1538-4357/](https://doi.org/10.3847/1538-4357/aa74e0)  
512 [aa74e0](https://doi.org/10.3847/1538-4357/aa74e0) doi: 10.3847/1538-4357/  
513 [aa74e0](https://doi.org/10.3847/1538-4357/aa74e0)
- 513 Chen, C. H. K., Leung, L., Boldyrev, S., Maruca, B. A., & Bale, S. D. (2014, Novem-  
514 ber). Ion-scale spectral break of solar wind turbulence at high and low beta.  
515 *Geophysical Research Letters*, 41(22), 8081–8088. Retrieved from [https://doi](https://doi.org/10.1002/2014gl062009)  
516 [.org/10.1002/2014gl062009](https://doi.org/10.1002/2014gl062009) doi: 10.1002/2014gl062009
- 517 Contel, O. L., Leroy, P., Roux, A., Coillot, C., Alison, D., Bouabdellah, A., ... de la  
518 Porte, B. (2014, September). The search-coil magnetometer for MMS. *Space Sci-*  
519 *ence Reviews*, 199(1-4), 257–282. Retrieved from [https://doi.org/10.1007/](https://doi.org/10.1007/s11214-014-0096-9)  
520 [s11214-014-0096-9](https://doi.org/10.1007/s11214-014-0096-9) doi: 10.1007/s11214-014-0096-9
- 521 Cranmer, S. R., Asgari-Targhi, M., Paz Miralles, M., Raymond, J. C., Strachan, L.,  
522 Tian, H., & Woolsey, L. N. (2015, May). The role of turbulence in coronal  
523 heating and solar wind expansion. *Philosophical Transactions of the Royal*  
524 *Society A: Mathematical, Physical and Engineering Sciences*, 373(2041),  
525 20140148. Retrieved from <https://doi.org/10.1098/rsta.2014.0148> doi:  
526 10.1098/rsta.2014.0148
- 527 Dudok de Wit, T., Alexandrova, O., Furno, I., Sorriso-Valvo, L., & Zimbardo, G.  
528 (2013, May). Methods for characterising microphysical processes in plasmas.  
529 *Space Science Reviews*, 178(2-4), 665–693. Retrieved from [https://doi.org/](https://doi.org/10.1007/s11214-013-9974-9)  
530 [10.1007/s11214-013-9974-9](https://doi.org/10.1007/s11214-013-9974-9) doi: 10.1007/s11214-013-9974-9
- 531 Ergun, R. E., Tucker, S., Westfall, J., Goodrich, K. A., Malaspina, D. M., Summers,  
532 D., ... Cully, C. M. (2014, December). The axial double probe and fields  
533 signal processing for the MMS mission. *Space Science Reviews*, 199(1-4),  
534 167–188. Retrieved from <https://doi.org/10.1007/s11214-014-0115-x> doi:  
535 10.1007/s11214-014-0115-x
- 536 Franci, L., Cerri, S. S., Califano, F., Landi, S., Papini, E., Verdini, A., ... Hellinger,  
537 P. (2017, November). Magnetic reconnection as a driver for a sub-ion-  
538 scale cascade in plasma turbulence. *The Astrophysical Journal*, 850(1),  
539 L16. Retrieved from <https://doi.org/10.3847/2041-8213/aa93fb> doi:  
540 10.3847/2041-8213/aa93fb
- 541 Franci, L., Landi, S., Matteini, L., Verdini, A., & Hellinger, P. (2015, October).  
542 HIGH-RESOLUTION HYBRID SIMULATIONS OF KINETIC PLASMA  
543 TURBULENCE AT PROTON SCALES. *The Astrophysical Journal*, 812(1),  
544 21. Retrieved from <https://doi.org/10.1088/0004-637x/812/1/21> doi:  
545 10.1088/0004-637x/812/1/21
- 546 Friedman, J. H. (1991, March). Multivariate adaptive regression splines. *The*  
547 *Annals of Statistics*, 19(1). Retrieved from [https://doi.org/10.1214/aos/](https://doi.org/10.1214/aos/1176347963)  
548 [1176347963](https://doi.org/10.1214/aos/1176347963) doi: 10.1214/aos/1176347963
- 549 Frisch, U. (1995). *Turbulence*. Cambridge University Press. Retrieved from <https://>

- doi.org/10.1017/cbo9781139170666 doi: 10.1017/cbo9781139170666
- Gingell, I., Schwartz, S. J., Burgess, D., Johlander, A., Russell, C. T., Burch, J. L., ... Wilder, F. (2017, November). MMS observations and hybrid simulations of surface ripples at a marginally quasi-parallel shock. *Journal of Geophysical Research: Space Physics*, *122*(11). Retrieved from <https://doi.org/10.1002/2017ja024538> doi: 10.1002/2017ja024538
- Gingell, I., Schwartz, S. J., Eastwood, J. P., Burch, J. L., Ergun, R. E., Fuselier, S., ... Wilder, F. (2019, February). Observations of magnetic reconnection in the transition region of quasi-parallel shocks. *Geophysical Research Letters*, *46*(3), 1177–1184. Retrieved from <https://doi.org/10.1029/2018gl081804> doi: 10.1029/2018gl081804
- Hollweg, J. V. (1999, July). Kinetic alfvén wave revisited. *Journal of Geophysical Research: Space Physics*, *104*(A7), 14811–14819. Retrieved from <https://doi.org/10.1029/1998ja900132> doi: 10.1029/1998ja900132
- Huang, S. Y., Hadid, L. Z., Sahraoui, F., Yuan, Z. G., & Deng, X. H. (2017, February). On the existence of the kolmogorov inertial range in the terrestrial magnetosheath turbulence. *The Astrophysical Journal*, *836*(1), L10. Retrieved from <https://doi.org/10.3847/2041-8213/836/1/110> doi: 10.3847/2041-8213/836/1/110
- Isenberg, P. A., & Hollweg, J. V. (1983). On the preferential acceleration and heating of solar wind heavy ions. *Journal of Geophysical Research*, *88*(A5), 3923. Retrieved from <https://doi.org/10.1029/ja088ia05p03923> doi: 10.1029/ja088ia05p03923
- Johlander, A., Schwartz, S., Vaivads, A., Khotyaintsev, Y. V., Gingell, I., Peng, I., ... Burch, J. (2016, October). Rippled quasiperpendicular shock observed by the magnetospheric multiscale spacecraft. *Physical Review Letters*, *117*(16). Retrieved from <https://doi.org/10.1103/physrevlett.117.165101> doi: 10.1103/physrevlett.117.165101
- King, J. H. (2005). Solar wind spatial scales in and comparisons of hourly wind and ACE plasma and magnetic field data. *Journal of Geophysical Research*, *110*(A2). Retrieved from <https://doi.org/10.1029/2004ja010649> doi: 10.1029/2004ja010649
- Kiyani, K. H., Osman, K. T., & Chapman, S. C. (2015, May). Dissipation and heating in solar wind turbulence: from the macro to the micro and back again. *Philosophical Transactions of the Royal Society A: Mathematical, Physical and Engineering Sciences*, *373*(2041), 20140155. Retrieved from <https://doi.org/10.1098/rsta.2014.0155> doi: 10.1098/rsta.2014.0155
- Klimchuk, J. A. (2006, March). On solving the coronal heating problem. *Solar Physics*, *234*(1), 41–77. Retrieved from <https://doi.org/10.1007/s11207-006-0055-z> doi: 10.1007/s11207-006-0055-z
- Kolmogorov, A. (1941, January). The Local Structure of Turbulence in Incompressible Viscous Fluid for Very Large Reynolds' Numbers. *Akademiia Nauk SSSR Doklady*, *30*, 301-305.
- Lalti, A., Khotyaintsev, Y. V., Dimmock, A. P., Johlander, A., Graham, D. B., & Olshevsky, V. (2022, August). A database of MMS bow shock crossings compiled using machine learning. *Journal of Geophysical Research: Space Physics*, *127*(8). Retrieved from <https://doi.org/10.1029/2022ja030454> doi: 10.1029/2022ja030454
- Lepping, R. P., Acuña, M. H., Burlaga, L. F., Farrell, W. M., Slavin, J. A., Schatten, K. H., ... Worley, E. M. (1995, February). The WIND magnetic field investigation. *Space Science Reviews*, *71*(1-4), 207–229. Retrieved from <https://doi.org/10.1007/bf00751330> doi: 10.1007/bf00751330
- Li, H., Jiang, W., Wang, C., Verscharen, D., Zeng, C., Russell, C. T., ... Burch, J. L. (2020, July). Evolution of the earth's magnetosheath turbulence: A statistical study based on MMS observations. *The Astrophysical Journal*,

- 605 898(2), L43. Retrieved from <https://doi.org/10.3847/2041-8213/aba531>  
 606 doi: 10.3847/2041-8213/aba531
- 607 Lindqvist, P.-A., Olsson, G., Torbert, R. B., King, B., Granoff, M., Rau, D.,  
 608 ... Tucker, S. (2014, November). The spin-plane double probe electric  
 609 field instrument for MMS. *Space Science Reviews*, 199(1-4), 137–165.  
 610 Retrieved from <https://doi.org/10.1007/s11214-014-0116-9> doi:  
 611 10.1007/s11214-014-0116-9
- 612 Matsumoto, Y., Amano, T., Kato, T. N., & Hoshino, M. (2015, February).  
 613 Stochastic electron acceleration during spontaneous turbulent recon-  
 614 nection in a strong shock wave. *Science*, 347(6225), 974–978. Retrieved from  
 615 <https://doi.org/10.1126/science.1260168> doi: 10.1126/science.1260168
- 616 Matthaeus, W. H., Wan, M., Servidio, S., Greco, A., Osman, K. T., Oughton, S., &  
 617 Dmitruk, P. (2015, May). Intermittency, nonlinear dynamics and dissipation  
 618 in the solar wind and astrophysical plasmas. *Philosophical Transactions of the*  
 619 *Royal Society A: Mathematical, Physical and Engineering Sciences*, 373(2041),  
 620 20140154. Retrieved from <https://doi.org/10.1098/rsta.2014.0154> doi:  
 621 10.1098/rsta.2014.0154
- 622 McComas, D., Bame, S., Barker, P., Feldman, W., Phillips, J., Riley, P., & Griffee, J.  
 623 (1998).  
 624 *Space Science Reviews*, 86(1/4), 563–612. Retrieved from [https://doi.org/](https://doi.org/10.1023/a:1005040232597)  
 625 [10.1023/a:1005040232597](https://doi.org/10.1023/a:1005040232597) doi: 10.1023/a:1005040232597
- 626 McKee, C. F., & Ostriker, E. C. (2007, September). Theory of star formation. *An-*  
 627 *nal Review of Astronomy and Astrophysics*, 45(1), 565–687. Retrieved from  
 628 <https://doi.org/10.1146/annurev.astro.45.051806.110602> doi: 10.1146/  
 629 annurev.astro.45.051806.110602
- 630 Milborrow, S., Hastie, T., & Tibshirani, R. (2011). earth: Multivariate adaptive re-  
 631 gression splines [Computer software manual]. Retrieved from [http://CRAN.R-](http://CRAN.R-project.org/package=earth)  
 632 [project.org/package=earth](http://CRAN.R-project.org/package=earth) (R package)
- 633 Ogilvie, K. W., Chornay, D. J., Fritzenreiter, R. J., Hunsaker, F., Keller, J., Lobell,  
 634 J., ... Gergin, E. (1995, February). SWE, a comprehensive plasma instrument  
 635 for the WIND spacecraft. *Space Science Reviews*, 71(1-4), 55–77. Retrieved  
 636 from <https://doi.org/10.1007/bf00751326> doi: 10.1007/bf00751326
- 637 Peredo, M., Slavin, J. A., Mazur, E., & Curtis, S. A. (1995). Three-dimensional  
 638 position and shape of the bow shock and their variation with alfvénic, sonic  
 639 and magnetosonic mach numbers and interplanetary magnetic field orien-  
 640 tation. *Journal of Geophysical Research*, 100(A5), 7907. Retrieved from  
 641 <https://doi.org/10.1029/94ja02545> doi: 10.1029/94ja02545
- 642 Phan, T. D., Eastwood, J. P., Shay, M. A., Drake, J. F., Sonnerup, B. U. O., Fu-  
 643 jimoto, M., ... Magnes, W. (2018, May). Electron magnetic reconnection  
 644 without ion coupling in earth’s turbulent magnetosheath. *Nature*, 557(7704),  
 645 202–206. Retrieved from <https://doi.org/10.1038/s41586-018-0091-5> doi:  
 646 10.1038/s41586-018-0091-5
- 647 Pollock, C., Moore, T., Jacques, A., Burch, J., Gliese, U., Saito, Y., ... Zeuch,  
 648 M. (2016, March). Fast plasma investigation for magnetospheric multiscale.  
 649 *Space Science Reviews*, 199(1-4), 331–406. Retrieved from [https://doi.org/](https://doi.org/10.1007/s11214-016-0245-4)  
 650 [10.1007/s11214-016-0245-4](https://doi.org/10.1007/s11214-016-0245-4) doi: 10.1007/s11214-016-0245-4
- 651 Ragot, B. R. (2022, March). Solar wind magnetic field correlation length: Correla-  
 652 tion functions versus cross-field displacement diffusivity test. *The Astrophysical*  
 653 *Journal*, 927(2), 182. Retrieved from [https://doi.org/10.3847/1538-4357/](https://doi.org/10.3847/1538-4357/ac281b)  
 654 [ac281b](https://doi.org/10.3847/1538-4357/ac281b) doi: 10.3847/1538-4357/ac281b
- 655 Russell, C. T., Anderson, B. J., Baumjohann, W., Bromund, K. R., Dearborn,  
 656 D., Fischer, D., ... Richter, I. (2014, August). The magnetospheric  
 657 multiscale magnetometers. *Space Science Reviews*, 199(1-4), 189–256.  
 658 Retrieved from <https://doi.org/10.1007/s11214-014-0057-3> doi:  
 659 10.1007/s11214-014-0057-3

- 660 Sahraoui, F., Goldstein, M. L., Belmont, G., Canu, P., & Rezeau, L. (2010, September)  
 661 ). Three dimensional Anisotropic Spectra of turbulence at subproton scales  
 662 in the solar wind. *Physical Review Letters*, *105*(13). Retrieved from [https://](https://doi.org/10.1103/physrevlett.105.131101)  
 663 [doi.org/10.1103/physrevlett.105.131101](https://doi.org/10.1103/physrevlett.105.131101) doi: 10.1103/physrevlett.105  
 664 .131101
- 665 Sahraoui, F., Hadid, L., & Huang, S. (2020, February). Magnetohydrodynamic  
 666 and kinetic scale turbulence in the near-earth space plasmas: a (short) biased  
 667 review. *Reviews of Modern Plasma Physics*, *4*(1). Retrieved from [https://](https://doi.org/10.1007/s41614-020-0040-2)  
 668 [doi.org/10.1007/s41614-020-0040-2](https://doi.org/10.1007/s41614-020-0040-2) doi: 10.1007/s41614-020-0040-2
- 669 Smith, C., L'Heureux, J., Ness, N., Acuña, M., Burlaga, L., & Scheifele, J. (1998).  
 670 *Space Science Reviews*, *86*(1/4), 613–632. Retrieved from [https://doi.org/](https://doi.org/10.1023/a:1005092216668)  
 671 [10.1023/a:1005092216668](https://doi.org/10.1023/a:1005092216668) doi: 10.1023/a:1005092216668
- 672 Stawarz, J. E., Eastwood, J. P., Phan, T. D., Gingell, I. L., Pyakurel, P. S., Shay,  
 673 M. A., ... Contel, O. L. (2022, January). Turbulence-driven magnetic reconnection  
 674 and the magnetic correlation length: Observations from magnetospheric  
 675 multiscale in earth's magnetosheath. *Physics of Plasmas*, *29*(1), 012302. Retrieved from <https://doi.org/10.1063/5.0071106> doi: 10.1063/5.0071106
- 676 Stawarz, J. E., Eastwood, J. P., Phan, T. D., Gingell, I. L., Shay, M. A., Burch,  
 677 J. L., ... Franci, L. (2019, June). Properties of the turbulence associated  
 678 with electron-only magnetic reconnection in earth's magnetosheath. *The Astrophysical Journal*, *877*(2), L37. Retrieved from [https://doi.org/10.3847/](https://doi.org/10.3847/2041-8213/ab21c8)  
 679 [2041-8213/ab21c8](https://doi.org/10.3847/2041-8213/ab21c8) doi: 10.3847/2041-8213/ab21c8
- 680 Torbert, R. B., Russell, C. T., Magnes, W., Ergun, R. E., Lindqvist, P.-A., LeContel,  
 681 O., ... Lappalainen, K. (2014, November). The FIELDS instrument suite on  
 682 MMS: Scientific objectives, measurements, and data products. *Space Science*  
 683 *Reviews*, *199*(1-4), 105–135. Retrieved from [https://doi.org/10.1007/](https://doi.org/10.1007/s11214-014-0109-8)  
 684 [s11214-014-0109-8](https://doi.org/10.1007/s11214-014-0109-8) doi: 10.1007/s11214-014-0109-8
- 685 Wang, R., Lu, Q., Nakamura, R., Baumjohann, W., Russell, C. T., Burch, J. L.,  
 686 ... Gershman, D. (2017, October). Interaction of magnetic flux ropes  
 687 via magnetic reconnection observed at the magnetopause. *Journal of Geophysical Research: Space Physics*, *122*(10), 10436–10447. Retrieved from  
 688 <https://doi.org/10.1002/2017ja024482> doi: 10.1002/2017ja024482
- 689 Yordanova, E., Vörös, Z., Raptis, S., & Karlsson, T. (2020, February). Current sheet  
 690 statistics in the magnetosheath. *Frontiers in Astronomy and Space Sciences*, *7*.  
 691 Retrieved from <https://doi.org/10.3389/fspas.2020.00002> doi: 10.3389/  
 692 fspas.2020.00002
- 693 Zhuravleva, I., Churazov, E., Schekochihin, A. A., Allen, S. W., Arévalo, P.,  
 694 Fabian, A. C., ... Werner, N. (2014, October). Turbulent heating in galaxy  
 695 clusters brightest in x-rays. *Nature*, *515*(7525), 85–87. Retrieved from  
 696 <https://doi.org/10.1038/nature13830> doi: 10.1038/nature13830